Inhomogeneous eigenmode localization, chaos, and correlations in large disordered clusters

Mark I. Stockman
Department of Physics and Astronomy, Georgia State University, Atlanta, Georgia 30303
(Received 6 May 1997)

Statistical and localization properties of dipole eigenmodes (plasmons) of fractal and random nonfractal clusters are investigated. The problem is mathematically equivalent to the quantum-mechanical eigenproblem for vector (spin-1) particles with a dipolar hopping amplitude in the same cluster. In fractal clusters, individual eigenmodes are singular on the small scale and their intensity strongly fluctuates in space. They possess neither strong nor weak localization properties. Instead, an inhomogeneous localization pattern takes place, where eigenmodes of very different coherence radii coexist at the same frequency. Chaotic behavior of the eigenmodes is found for fractal clusters in the region of small eigenvalues, i.e., in the vicinity of the plasmon resonance. The observed chaos is ''stronger'' than for quantum-mechanical problems on regular sets in the sense that the present problem is characterized by (deterministically) chaotic behavior of the amplitude correlation function (dynamic form factor). This chaotic behavior consists of rapid changes of the phase of the amplitude correlation in spatial and frequency domains, while its magnitude is a very smooth function. A transition between the chaotic and scaling behavior with increase of eigenvalue is observed. In contrast to fractal clusters, random clusters with nonfractal geometry do not exhibit chaotic behavior, but rather a mesoscopic delocalization transition of the eigenmodes with decrease of eigenvalue. [S1063-651X(97)01112-4]

PACS number(s): 05.45.+b, 71.45.Gm, 78.20.Bh, 61.43.Hv,

I. INTRODUCTION

The problem of properties of disordered systems is of universal significance in physics. There is a wide class of mutually related phenomena associated with disorder. Among those phenomena are localization of elementary excitations (quasiparticles and eigenmodes), fluctuations and enhancement of local fields, correlation of such fluctuations, and spatial-temporal chaos, including quantum chaos. In turn, the correlation of fluctuations is related to the linear response function of a system by the fluctuation-dissipation theorem [1]. In this paper we consider localization, spatially correlated fluctuations, and chaos of polar eigenmodes (traditionally called ''plasmons'') of large disordered clusters. This problem maps (i.e., it is mathematically equivalent) to a tight-binding eigenproblem for the Schrödinger equation for a vector (spin-1) particle.

Of the phenomena mentioned above, electron localization is responsible, in particular, for Anderson's metal-insulator transitions [2]. A similar phenomenon of importance for us is localization of plasmons. Such a localization is intimately related to fluctuations and enhancement of local electromagnetic fields in disordered systems, which cause surface-enhanced Raman scattering from surfaces [3] and fractal clusters [4], and giant enhancement of nonlinear-optical responses of such clusters [5]. Physically, the localization of plasmons is of principal importance for the optical-response enhancement because it is a near-zone analog of focusing of electromagnetic radiation (or it is a counterpart of the creation of speckles by scattering of light waves from a random object). The ''focusing'' (or creation of speckles) of electromagnetic fields by plasmon localization occurs on a nanometer scale rather than on a micrometer scale as in conventional optical far-zone focusing. A near-zone focusing, similar to a far-zone optical focusing, creates local regions of high-field intensity, causing enhancement of nonlinear photoprocesses. Note that localization of plasmons in disordered fractal clusters and creation of nanoregions of high local-field intensity (speckles) have been experimentally observed with the use of a photon scanning tunneling microscope [6]. Similar to the conventional focusing, the nonlinear-optical enhancement due to the plasmon localization is stronger the higher the order of nonlinearity [7].

Because of the mutual mapping of a plasmon eigenproblem and the corresponding quantum eigenproblem, another field of relevance for the class of phenomena under consideration is quantum chaos, which mathematically is chaos in solutions (we will call them interchangeably eigenfunctions or eigenvectors) of the corresponding linear eigenproblems (Schrödinger-type equations). Among many properties of quantum chaos, the most relevant for the present paper are real-space localization and spatial correlations of eigenvectors. A partial localization of chaotic eigenfunctions is manifested by their scarring [8,9]. Related properties are spatial correlations of the probability amplitudes (eigenfunctions) and probability densities. A seminal paper by Berry [10] conjectured that the Wigner density matrix for a nonintegrable chaotic system respects a microcanonical distribution. As a result, the spatial correlation function behaves as the Bessel function $j_1(kr)$, resulting in a power-law decay proportional to $1/r$. Thus no long-range spatial correlation of wave functions should exist. The absence of long-range spatial correlation in chaotic systems with time reversal (without a magnetic field) has been confirmed analytically by Fal'co and Efetov using the supersymmetric σ model. Note that in the presence of an intermediate-strength magnetic field (that is, in the crossover region between orthogonal and unitary classes) weak long-range spatial correlation for electrons is predicted [11]. The widely used random matrix theory of quantum chaos also does not include the long-range spatial correlations. In contrast to the above theories that are applicable to massive particles moving in potential fields, we will

 © 1997 The American Physical Society

show below that in our case there are long-range spatial correlations present in correlation functions of both amplitude and probability (intensity).

We consider both fractal (self-similar) and nonfractal geometries of clusters. There exists some understanding of localization of eigenmodes in self-similar (fractal) systems. A nontrivial geometry of localized eigenmodes described by a multifractal statistics [12] has been established recently for vibrations of fractals (''fractons'') [13–16]. Localized vibrational excitations of fractal drums at low frequencies have been found [17]. The polar excitations (plasmons) that are considered in the present paper differ significantly from vibrations mentioned above. We demonstrate below that the polar excitations exhibit a highly singular behavior throughout the spectral region. In contrast, for instance, the vibrational excitations of fractal drums are multifractal only for large enough wavelengths (low frequencies) [17], where they can ''feel'' the fractal boundary of the drum. Related but opposite behavior is typical for nonpolar waves in locally disordered media, i.e., media with short-length correlation of the disorder. In this case, as soon as the wavelength exceeds the correlation length of the disorder, the excitation ''sees'' an almost uniform medium and propagates with little scattering (the Anderson transition).

Intrinsically, polar excitations in a disordered medium are principally different from nonpolar modes because they create charges throughout the medium, causing an infinite (or a very long) range of interaction. This results in differences in spectra: Polar excitations have spectral gap, i.e., they are non-Goldstonian excitations, different from, say, acoustic-type vibrations [18]. Earlier we formulated a hypothesis that the polar excitations of fractal clusters are strongly localized [19]. This implies that there exists only one spatial scale characterizing the excitation that plays the role of wavelength and total localization length of the cluster simultaneously. This hypothesis was formulated analogously to Alexander and Orbach's strong-localization hypothesis for vibrations [20]. However, the theoretical prediction of Ref. [19] did not agree with our subsequent results of more detailed and higher-resolution numerical simulations [21]. Later we found that polar eigenmodes of fractals clusters do not follow familiar behavior of strong or weak localization [22]. Instead, these eigenmodes respect a new pattern that we call inhomogeneous localization, where eigenmodes of very different localization lengths, from the typical nearest-neighbor distance R_0 (the minimum scale) to the total size of the cluster R_c (the maximum scale), coexist at any given frequency frequency in a very wide spectral range [22]. The pattern of inhomogeneous localization is supported by extensive numerical investigation of this paper.

Polar excitations of clusters are traditionally called ''surface plasmons.'' It is implied that the wavelength λ of the exciting electromagnetic radiation greatly exceeds the total size of the cluster R_c. In a spherical particle, the surface plasmon is described by a spatially uniform polarization extended over the whole sphere, oscillating harmonically in time. This polarization creates charges only at the surface of the particle, thus justifying the name surface plasmon. As we have found and present in this paper, in contrast to the behavior of surface plasmons in regular spherical particles, for the whole spectral region the polar excitations of a large self-similar (fractal) cluster fill in the whole space of the cluster only on average. Each particular eigenmode is extremely nonuniform. Consequently, it creates charges throughout the volume of a cluster causing long-range interactions. For these reasons, we will call the polar excitations of disordered clusters plasmons, omitting the term ''surface'' as inadequate.

The investigation in the present paper is aimed at understanding spatial behavior of the eigenmodes of the dipolar eigenproblem (or eigenfunctions of the equivalent quantum-mechanical vector eigenproblem) defined below in Sec. II A. We obtain and discuss numerical data of four types. First, we consider individual eigenmodes (Sec. III B). We show that that the eigenmodes of fractal clusters are chaotic, with highly random and singular distributions of polarization (or quantum-mechanical amplitude). The eigenmodes change dramatically with small changes of their frequencies (eigenvalues), which is another signature of chaos. We also show that not only individual eigenmodes but also local fields created by external waves are chaotic and highly singular. This chaos and singularity are undoubtedly responsible for the giant fluctuations of local fields and nonlinear-optical enhancement found earlier [7].

The other three groups of results deal with data averaged statistically yielding various distribution and correlation functions introduced in Sec. II B. This statistical averaging is done in two steps: over many eigenmodes belonging to a relatively narrow spectral region in the vicinity a given frequency for a single cluster and then over a large ensemble of clusters. Specifically, the second group of data deals with statistical measures of the eigenmode localization (Sec. III C). It is based on the distribution function $P(L,X)$, where L is the localization length and X is an eigenvalue of the problem that is uniquely related to the physical frequency $\omega=\omega(X)$; see Sec. II A. We show in particular that for fractal clusters this distribution is very wide. In view of its width, the average localization length at a given frequency L_X (''dispersion relation'') is not nearly sufficient to characterize the distribution. A boundary of the distribution $P(l,X)$ has scaling form and the whole distribution obeys scaling dependence as a consequence of clusters' self-similarity. For nonfractal random clusters, the function $P(L,X)$ indicates a delocalization transition of the eigenmodes as frequency decreases $(X\rightarrow 0)$.

The third group of data deals with the correlation function $S(\mathbf{r},X)$ of the eigenmode amplitudes at two spatial points separated by a distance $\mathbf{r}$ at a frequency $\omega(X)$, averaged over a narrow interval of frequencies and over an ensemble of clusters (Sec. III D). This correlation function is called synonymously the dynamic form factor of a system. It is related to the imaginary part of the system's polarizability and also describes different physical phenomena including energy losses of charged particles and equilibrium fluctuations of electromagnetic fields (as described by the fluctuation-dissipation theorem) [1]. In addition, the dynamic form factor contains other physical information on a system including, but not limited to, dispersion of different branches of elementary excitations and localization-delocalization transitions of these excitations. As found below in Sec. III D, for fractal clusters, the dynamic form factor exhibits a nonuniform, quasichaotic (''turbulent'') pattern in the coordinate-

frequency domain. This chaotic behavior appears abruptly (as in a phase transition) as eigenvalue X [and frequency $\omega(X)$] decreases and, correspondingly, the correlation length of the eigenmodes increases. At the point of the transition, pronounced binary and ternary branches disappear, replaced by chaotic behavior. In a sense, the chaos found is stronger than the chaos predicted by Berry [10], since not only individual eigenvectors but also their dynamic form factor are chaotic. Also in contrast to Ref. [10], the correlation of amplitudes is long range, extending over the whole volume of the clusters, in agreement with the above-mentioned data on the localization-length distribution. In contrast to fractals, for random nonfractal clusters the behavior of the dynamic form factor is predominantly nonchaotic, dominated by binary and ternary branches disappearing at the point of a mesoscopic delocalization transition as $X\rightarrow 0$.

The fourth group of data deals with the correlation function $C(\mathbf{r},X)$ of the eigenmode intensities (probability densities for the corresponding quantum eigenproblem) at two points separated by a distance $\mathbf{r}$ for eigenvalues close to X (Sec. III E). Different from the dynamic form factor, the intensity correlation function is insensitive to relative phases of the eigenvectors, but is sensitive to their intensities (probabilities). This is one of the correlation functions studied for quantum-chaos electronic problems in Ref. [11] with the conclusion that there are no long-range spatial correlations in the absence of a magnetic field. In contrast, we find for our problem that there are such correlations extended over the whole available volume of system. Distinct from the dynamic form factor $S(\mathbf{r},X)$, the correlation function $C(\mathbf{r},X)$ is smooth in the whole spectral region. This implies that the fluctuations causing the turbulent behavior of the dynamic form factor are associated with phases of the cluster plasmons, while their intensities on average have a smooth, regular second-order correlator. Finally, we show that this intensity-correlation function $C(\mathbf{r},X)$ obeys a scaling relation with a very high accuracy. This implies that there is only one significant length scale in the problem and that it is the whole size of the system R_c. This property is certainly due to the long range of the interaction and to self-similarity of the clusters. This scaling behavior is one of the signatures of the inhomogeneous localization of the eigenmodes (cluster plasmons).

With regard to the analytical part of the paper, in Sec. II we present the necessary relations in the spectral representation. In particular, we introduce relevant correlation functions and predict their scaling (Sec. II B) and we obtain simple predictions within the framework of a binary approximation (Sec. II C). Section III is devoted to numerical investigation (discussed above in the Introduction).

II. BASIC RELATIONS

A. Spectral representation and linear response

For the sake of completeness, in this section we will briefly summarize spectral theory [19] of the dipolar response of clusters and also introduce necessary definitions and relations. Consider a cluster consisting of N constituent particle (called below monomers) positioned at points $\mathbf{r}_i$, $i=1,\ldots,N$. The monomers are subjected to an external-wave electric field (the field at an ith monomer is $\mathbf{E}_i^{(0)}$) oscillating at an optical frequency. This field polarizes monomers, inducing oscillating dipole moments $\mathbf{d}_i$, which are random quantities due to the random structure of the cluster. We assume that the radius of the cluster is much smaller than the wavelength of the optical radiation $R_c \ll \lambda$. Then the induced dipole moments obey a well-known system of equations

$$Zd_{i\alpha}=E_i^{(0)}-\sum_{j=1}^{N} W_{i\alpha,j\beta}d_{j\beta}, \tag{1}$$

where $Z=\alpha_0^{-1}$, α_0 is the dipole polarizability of an isolated monomer, greek letters in subscripts denote vector indices $(\alpha,\beta,\ldots=x,y,z)$, with the summation over the repeated indices implied, W is the dipole-interaction tensor

$$W_{i\alpha,j\beta}=\begin{cases}[r_{ij}^2\delta_{\alpha\beta}-3(r_{ij})_\alpha(r_{ij})_\beta]r_{ij}^{-5}, & i\neq j\\ 0, & i=j,\end{cases} \tag{2}$$

and $\mathbf{r}_{ij}\equiv\mathbf{r}_i-\mathbf{r}_j$.

Introducing a $3N$-dimensional vector $|d)$ with the components $(i\alpha|d)=d_{i\alpha}$ (and similar for other vectors), we obtain a single equation in a $3N$-dimensional space [18,19]

$$(Z+W)|d)=|E_0), \tag{3}$$

where the dipole-interaction operator is defined by its matrix elements as $(i\alpha|W|j\beta)=W_{i\alpha,j\beta}$. Similar to Ref. [19], we introduce the spectral variable $X=-\mathrm{Re}Z$ that will be used instead of the frequency and a parameter $\varepsilon=-\mathrm{Im}Z$, which determines dissipation in a monomer. The main advantage of spectral theory is the separation of the geometrical and material properties of a system. The latter enter the theory only through the parameter Z, while geometry is taken into account by eigenvectors of Eq. (3). In particular, frequency ω is a function (though not necessarily a single-valued function in the whole spectral region) of X defined by the relation $X=-\mathrm{Re}\alpha_0^{-1}(\omega)$.

The solution of Eq. (2) is determined by the eigenvalues w_n and eigenvectors (eigenmodes) $|n)$ of the W operator [19],

$$(W-w_n)|n)=0, \tag{4}$$

where $n=1,\ldots,3N$ is the eigenmode's number. These eigenmodes are the plasmons discussed in Sec. I. Equation (4) has the form of a Schrödinger equation for vector (spin 1) particles on a lattice $\{\mathbf{r}_i\}$, where $|n)$ are stationary wave functions. Thus the present results are valid also for the corresponding quantum vector problem. The projection $(i\alpha|n)$ is the amplitude of an nth eigenmode at an ith particle with a polarization α or the quantum-mechanical amplitude for a vector particle at the ith node with polarization α.

The solution of Eq. (3) in terms of spectral representation is

$$d_{i\alpha}=\sum_j \mathcal{G}_{i\alpha,j\beta}E_{j\beta}^{(0)}, \tag{5}$$

where $\mathcal{G}$ is the Green's function

$$\mathcal{G}_{i\alpha,j\beta}=\left\langle i\alpha\left|\frac{1}{Z+W}\right|j\beta\right\rangle=\sum_n (i\alpha|n)(j\beta|n)(Z+w_n)^{-1}. \tag{6}$$

The polarization $\mathbf{P}(\mathbf{r})$ is given by the conventional formula [1] $P_\alpha(\mathbf{r})=\int\chi_{\alpha\beta}(\mathbf{r},\mathbf{r}')E^{(0)}_\beta(\mathbf{r}')d^3r'$. For a composite consisting of the clusters, the susceptibility $\chi_{\alpha\beta}(\mathbf{r},\mathbf{r}')$ is expressed in terms of the Green's function as

$$\chi_{\alpha\beta}(\mathbf{r},\mathbf{r}')=\left\langle\sum_{i,j}\mathcal{G}_{i\alpha,j\beta}\delta(\mathbf{r}-\mathbf{r}_i)\,\delta(\mathbf{r}'-\mathbf{r}_j)\right\rangle, \tag{7}$$

where the angular brackets denote ensemble averaging over clusters, including their positions and orientation. For a composite consisting of randomly positioned clusters, the polarizability obviously depends only on the difference of coordinates,

$$\alpha_{\alpha\beta}(\mathbf{r},\mathbf{r}')=\alpha_{\alpha\beta}(\mathbf{r}-\mathbf{r}')=\left\langle\sum_{i,j}\mathcal{G}_{i\alpha,j\beta}\delta(\mathbf{r}-\mathbf{r}_{ij})\right\rangle. \tag{8}$$

The susceptibility (7) in this case is $\chi_{\alpha\beta}(\mathbf{r},\mathbf{r}')=n\alpha_{\alpha\beta}(\mathbf{r}-\mathbf{r}')$, where n is the concentration of clusters in the composite.

B. Correlation and distribution functions

The dynamic form factor $S_{\alpha\beta}(\mathbf{r},X)$ is defined as the correlation function of polarization amplitudes $(i\alpha|n)$ and $(j\beta|n)$ at two points $\mathbf{r}_i$ and $\mathbf{r}_j$, separated by a given distance $\mathbf{r}=\mathbf{r}_i-\mathbf{r}_j$ for eigenvectors $|n)$ with eigenvalues w_n close to the given value of X. Namely,

$$\begin{aligned}S_{\alpha\beta}(\mathbf{r},X)&=\frac{1}{\pi}\mathrm{Im}\alpha_{\alpha\beta}(X,\mathbf{r})\\&=\left\langle\sum_{n,i,j}(i\alpha|n)(j\beta|n)\,\delta(X-w_n)\,\delta(\mathbf{r}-\mathbf{r}_{ij})\right\rangle,\end{aligned} \tag{9}$$

where we also indicate the relation between the form factor and the polarizability $\alpha_{\alpha\beta}$ (in establishing this relation, we neglect the spectral width ε compared to X). The same form factor defines also the correlation of the equilibrium fluctuations of the polarization in the composite, in accord with the fluctuation-dissipation theorem [1].

Similarly, we introduce the second-order correlator $C(\mathbf{r},X)$, i.e., the correlation function of the eigenmode intensities $(i\alpha|n)^2$ and $(j\beta|n)^2$,

$$C(\mathbf{r},X)=\left\langle\sum_{n,i,j}(i\alpha|n)^2(j\beta|n)^2\,\delta(X-w_n)\,\delta(\mathbf{r}-\mathbf{r}_{ij})\right\rangle. \tag{10}$$

The correlators of Eqs. (9) and (10) are normalized in the following way:

$$\int_{-\infty}^{\infty}S_{\alpha\beta}(\mathbf{r},X)\,dX=N\delta_{\alpha\beta}\delta(\mathbf{r}), \tag{11a}$$

$$\int C(\mathbf{r},X)d^3r=\nu(X), \tag{11b}$$

where ν is the spectral density of eigenmodes $\nu(X)=\Sigma_n\delta(X-w_n)$. Equation (11a) is obviously equivalent to the dipole sum rule. The polarizability (8) for a single cluster satisfies the optical theorem

$$S_{\alpha\beta}(\mathbf{r},X)=\frac{\varepsilon}{\pi}\int\alpha^*_{\alpha\mu}(\mathbf{r}-\mathbf{r}')\alpha_{\mu\beta}(\mathbf{r}')d^3r' \tag{12}$$

that follows from the orthonormality and closure of the vector set $|i\alpha)$. We used this relation to independently check results of numerical computations. We also note that the function $G_X(r)$ introduced in Ref. [22] is related to Eq. (10) by $G_X(r)=C(r,X)/\nu(X)$.

A useful parameter to characterize the localization of an nth eigenmode is its localization radius L_n defined as the gyration radius for the eigenmode's intensities,

$$L_n^2=\sum_i r_i^2(i\beta|n)^2-\left[\sum_i\mathbf{r}_i(i\beta|n)^2\right]^2. \tag{13}$$

Apart from the distributions of Eqs. (9) and (10), we also introduce the distribution $P(L,X)$ of the localization lengths at a given frequency $\omega(X)$, namely,

$$P(L,X)=\left\langle\sum_n\delta(L-L_n)\,\delta(X-w_n)\right\rangle. \tag{14}$$

This distribution is normalized similar to Eq. (11b), $\int P(L,X)dL=\nu(X)$. The average localization length L_X at a given X can be expressed in the equivalent forms

$$\begin{aligned}L_X^2&=\left\langle\sum_n L_n^2\delta(X-w_n)\right\rangle\Big/\,\nu(X)\\&=\int_{-\infty}^{\infty}P(L,X)L^2dL\Big/\,\nu(X)\\&=\frac{1}{2}\int r^2C(r,X)d^3r\Big/\,\nu(X).\end{aligned} \tag{15}$$

This length as a function of X plays the role of the ''dispersion relation'' of excitations in the clusters (cf. Refs. [18] and [21]).

For self-similar (fractal) clusters there is no characteristic size except for the minimum size (the distance between nearest monomers R_0) and the maximum scale (the total size of the cluster R_c). Because the interaction is very long range, for distances $r\gg R_0$ the minimum size should not be relevant. On the other hand, for the same reason, the total size of a cluster R_c may be an essential parameter. Therefore, one can expect scaling of the correlation and distribution functions with R_c, namely,

$$S(r,X)=\mathcal{S}\left(\frac{r}{R_c},X\right), \tag{16a}$$

$$C(r,X)=\mathcal{C}\left(\frac{r}{R_c},X\right), \tag{16b}$$

$$P(L,X)=\mathcal{P}\left(\frac{L}{R_c},X\right), \tag{16c}$$

where $\mathcal{S}$, $\mathcal{C}$, and $\mathcal{P}$ are functions whose first argument is dimensionless and of order 1 or less. If the maximum scale R_c is also not relevant (possibly due to a strong dynamic screening), one expects a power-law form of the corresponding functions

$$S(r,X)\propto r^s, \tag{17a}$$

$$C(r,X)\propto r^c, \tag{17b}$$

$$P(L,X)\propto L^p, \tag{17c}$$

where s, c, and p are the corresponding scaling indices. Because the frequency parameter X enters the basic equations (1) and (3) only in a combination with the cube of the radius, then necessarily the indices should not depend on the frequency (parameter X).

C. Binary approximation

The correlation functions introduced above cannot be calculated analytically in the general case. Here we will employ the binary approximation [19] to calculate $S(r,X)$. The binary approximation assumes that each of the contributing eigenmodes is concentrated in two small regions separated by some distance $\boldsymbol{\rho}$. In that case the eigenmode equation (4) can be solved exactly.

For a given pair of localization regions, the solution yields six eigenmodes. There are two longitudinal modes, i.e., modes where the direction of the oscillating dipoles coincides with $\boldsymbol{\rho}$. Denoting these modes as $|z\pm)$, one gets the corresponding eigenvalues and the localization amplitudes as

$$w_{z\pm}=\pm\frac{2}{\rho^3},\quad (z\pm|1\alpha)=\frac{n_\alpha}{\sqrt{2}},\quad (z\pm|2\alpha)=\mp\frac{n_\alpha}{\sqrt{2}}, \tag{18}$$

where $\mathbf{n}=\boldsymbol{\rho}/\rho$. There are also four transverse eigenmodes $|x\pm)$ and $|y\pm)$, with the eigenvalues and localization amplitudes

$$w_{x\pm}=w_{y\pm}=\pm\frac{1}{\rho^3},\quad (x\pm|1\alpha)=\frac{n_\alpha^{(x)}}{\sqrt{2}},\quad (x\pm|2\alpha)=\pm\frac{n_\alpha^{(x)}}{\sqrt{2}}, \tag{19}$$

and similarly for $|y\pm)$, where $\mathbf{n}^{(x)}$ and $\mathbf{n}^{(y)}$ are normal unit vectors in the plane perpendicular to the direction of $\boldsymbol{\rho}$. Substituting Eqs. (18) and (19) into Eq. (9) and taking into account that in this case $\boldsymbol{\rho}=\mathbf{r}_{ij}$, we obtain for the dynamic form factor $S(r,X)=\frac{1}{3}S_{\alpha\alpha}(r,X)$,

$$S(r,X)=\delta(r)\,\nu(x)+f(r)\left[\delta\left(X+\frac{2}{r^3}\right)-\delta\left(X-\frac{2}{r^3}\right)+2\,\delta\left(X-\frac{1}{r^3}\right)-2\,\delta\left(X+\frac{1}{r^3}\right)\right], \tag{20}$$

where $f(r)=N\langle\delta(r-\rho)\rangle$ is the distribution function of the distance ρ, a smooth regular function.

To interpret Eq. (20) let us consider, e.g., the spectral detuning to the red from the plasmon resonance. For metallic clusters this is the most interesting case because the light frequency is in the visible range. In this case $X<0$ and Eq. (20) shows that at small r there is a band of self-correlation that does not depend on X, i.e., is parallel to the X axis, described by the first δ function in Eq. (20). As r increases, this band is followed by a narrow negative-correlation band described by $X=-1/r^3$, followed by another narrow band with positive correlation described by

$$X=-\frac{2}{r^3}. \tag{21}$$

The first correction to the binary approximation is the ternary approximation, where an eigenmode is constituted not by two but by three excited regions separated by distances much larger than their sizes (similar to what is shown in the right lower panel of Fig. 1). Consider, for instance, a completely aligned symmetric mode, where the three excited regions are center-symmetrically positioned along a straight line. Such modes at a given total size ρ yield six different eigenvalues, where three of them are twice degenerate (denoted by $\otimes 2$),

$$w_n=-\frac{1}{\rho^3}\otimes 2,\quad \frac{2}{\rho^3},\quad \frac{1}{\rho^3}(-1\pm\sqrt{57}),\quad \frac{1}{2\rho^3}(1\pm\sqrt{57})\otimes 2. \tag{22}$$

The largest-magnitude eigenmode will manifest itself in the dynamic form factor for $X<0$ as a band of positive correlation given by the equation

$$X=-\frac{1}{r^3}(1+\sqrt{57}). \tag{23}$$

Below, we will compare the simple picture predicted by binary-ternary approximation to the results of numerical computations.

III. NUMERICAL RESULTS

A. Procedures

Numerical calculations have been made using cluster-cluster aggregate (CCA) clusters generated similarly to Refs. [23] and [24]. Random lattice gas (RLG) clusters also have been used to elucidate the relative roles of disorder and fractality. Clusters of both types are generated on a rectangular $100\times100\times100$ lattice. The RLG clusters are generated by randomly placing monomers within a sphere whose radius is chosen in such a way that these clusters have the same gyration radius as the CCA clusters with the same number of monomers to allow for direct comparison. Clusters of sizes $N=1500$ and $N=500$ have been used to test the scaling predicted by Eqs. (16).

The solution procedure consists in using the spectral expansion technique as described above in Sec. II A. The diagonalization of the dipole-dipole interaction matrix has been performed using the well-known Lanczos algorithms

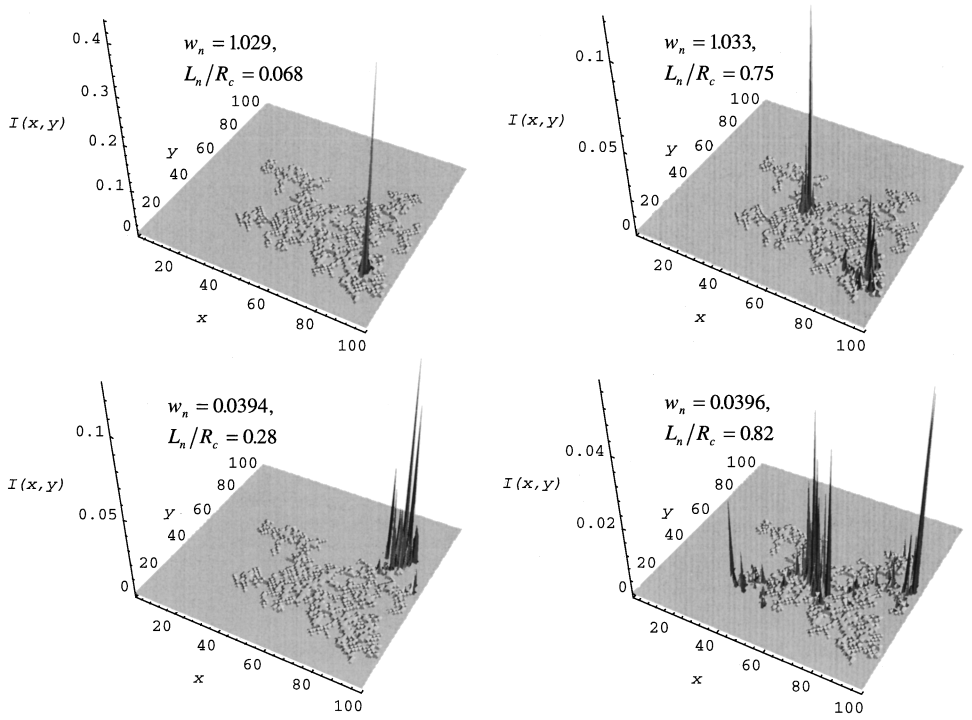

FIG. 1. Spatial distribution of the local-field intensities for an individual $N=1500$ CCA cluster shown over a two-dimensional projection of the cluster for the values of w_n indicated. The coordinates are shown in units of the lattice spacing R_0. The values of w_n are in units of R_0^{-3}. The value of the gyration radius L_n of the eigenmodes is shown relative to the cluster radius R_c.

for large matrix diagonalization [25]. The number of $N=1500$ clusters used in the accumulation of the Monte Carlo statistics is 300, and for $N=500$ it is 2000. Good statistical convergence has been found for all quantities calculated.

B. Local fields and localization of individual plasmons

We will first consider local fields of individual eigenmodes (plasmons) in the system. An example of local-field intensity distributions for four chosen eigenmodes of a CCA cluster is shown in Fig. 1. Features of these distributions are quite remarkable. First, the distributions change dramatically even for a small change of the eigenvalues w_n. In particular, the upper left distribution at $w_n=1.029$ is extremely localized, with the localization radius L_n of only $0.068R_c$. In contrast, just a few tenth of 1 % change of the eigenvalue to $w_n=1.033$ brings about a dramatic increase of the localization radius that makes it comparable with the total size $L_n=0.75R_c$ (see the upper right panel). However, this delocalized mode at $w_n=1.033$ is not uniform. To the opposite, it is formed by two sharp peaks (''hot spots''). These peaks correspond to coupled dipoles that oscillate coherently, as assumed in the binary approximation (see Sec. II C). The above-described strong and random variations of eigenvectors (eigenfunctions) even for next or very close eigenvalues is one of the most intuitive signatures of (quantum) chaos.

A situation similar in many respects occurs for the low-w_n part of the spectrum (see the lower panels in Fig. 1), i.e., in the vicinity of the plasmon resonance in isolated monomers. The difference from the case above is that the individual groups of peaks are wider. Nevertheless, the intensity distribution inside the peaks is highly singular and nonuniform, consisting of hot spots fluctuating in space and oscillating in time with coherent phases.

The behavior described above is in agreement with our previous findings of inhomogeneous localization [22]. However, the present findings disagree with our original hypothesis of strong localization [19] that implies that the eigenmodes in most of the spectrum should have small localization radii $L_n \ll R_c$. The numerical results presented above, along with the results that will be described below, show that the related numerical findings of Ref. [26] supporting the strong localization hypothesis are indeed incorrect. (All the eigenvectors shown and discussed in Ref. [26] have very small localization radii.

Let us consider now spatial distributions of the local field intensity at a given monomer $I_i=d_{i\alpha}^2$ [see Eq. (5)] for the case of excitation by an *external* field. An example of such a distribution is shown in Fig. 2 for two frequencies (parameter X) that are very close to each other and two perpendicular linear polarizations. These distributions are also extremely singular and fluctuating in space, even between the nearest-neighbor monomers. This property of the local fields is the reason underlying the giant fluctuations of the local fields found earlier [7]. The overall width of the distribution is of the order of the total cluster size. This is explained by the fact that the external radiation at a given frequency excites a group of individual eigenmodes, within which there always are delocalized modes. Because the interaction is very long ranged *and* the clusters are self-similar, there is no intrinsic length scale characteristic of the problem. Consequently, the spatial extent of the intensity distribution is limited only by the clusters' size.

A change of polarization of the exciting radiation at a given frequency brings about a dramatic redistribution of

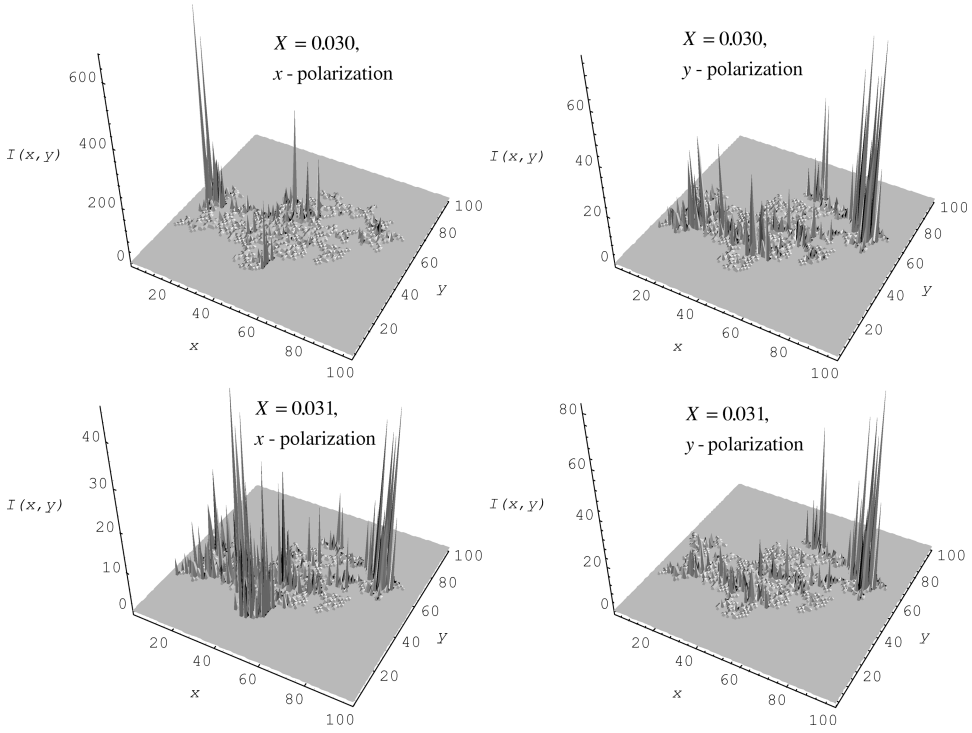

FIG. 2. Spatial distribution of the local-field intensities for external excitation of an individual $N=1500$ CCA cluster for the values of the frequency parameter X and polarizations of the exciting radiation shown. The value of the dissipation parameter $\varepsilon=10^{-3}R_0^{-3}$.

local intensities and change in the maximum intensities (cf. the left and right distributions in Fig. 2). The physical reason for this is that the resonant configurations of the monomers in most cases are highly anisotropic. This explains the high selectivity of the cluster photomodification in the radiation polarization observed experimentally [27]. The change of frequency of the exciting radiation by less than 1% also brings about pronounced changes in the intensity spatial distributions (cf. upper and lower panels in Fig. 2).

Generally, the observed intensity distributions are in a good qualitative agreement with the recent direct experimental observation by Moskovits and co-workers of the near-field optical fields in large silver clusters [6]. (A quantitative comparison is not possible because the distributions for individual clusters are inherently chaotic, strongly fluctuating from one cluster to another.) However, the conclusion of Ref. [6] that the observed phenomena support the strong localization hypothesis contradicts the conclusions of the present paper. We have commented that the observations of Ref. [6] do not support its strong localization conclusions [28,29]. In fact, these observations do support the inhomogeneous localization picture described in this paper, incompatible with the strong localization.

The patterns of the local fields discussed above show that the inhomogeneous localization scenario of polar excitations (plasmons) in large self-similar clusters is principally distinct from both the strong- and weak-localization scenarios of nonpolar excitations. The above-discussed individual eigenvectors (eigenstates) are chaotic. Consequently, they are difficult to compare quantitatively with each other. Therefore, we consider below the statistical characteristics (measures) of the eigenvectors.

C. Localization-length distributions

The distribution of the localization lengths of Eq. (14) calculated for an ensemble of $N=1500$ CCA clusters is shown in Fig. 3. The most conspicuous feature of this distribution is its very large width. This width extends from almost $2R_g$ (where $R_g\approx 40$, the mean gyration radius of the clusters) to some minimum cutoff size l_X that is a function of frequency $\omega(X)$. The cutoff is clearly seen in Fig. 3, where it is also indicated in the lower panel by a thick dashed line.

The distribution width is so large that the characterization of the distribution $P(L,X)$ by a single dispersion relation (15) is absolutely insufficient. For most of the spectral region, the cutoff length l_X by magnitude is intermediate between the maximum and minimum scales $R_0 \ll l_X \ll R_c$. This, along with the self-similarity of the clusters, suggests that l_X scales with X, i.e., $l_X \propto l^{\lambda}$. Indeed, Fig. 3 supports the possibility of such a scaling with the corresponding index $\lambda \approx -0.25$. We have also verified that the distribution $P(L,X)$ obeys with high accuracy the scaling relation (16c) (data not shown).

Another characteristic feature of the distribution shown in Fig. 3 is the presence of a narrow ridge seen in the lower panel between at $X\approx 1$ and 3. In this region, the distribution function scales as the approximately equidistant isolines suggest, in accord with Eq. (17c) with $p\approx -3$. The presence of such a scaling region, albeit a narrow one, indicates that the eigenmodes for $X\approx 1-3$ tend to be more localized and screened. Therefore, the maximum scale does not affect the distribution and power-law scaling takes place. We will return to the discussion of this region below in Sec. III D.

The clusters considered above are disordered and self-similar (fractal). It is interesting to separate effects of disor-

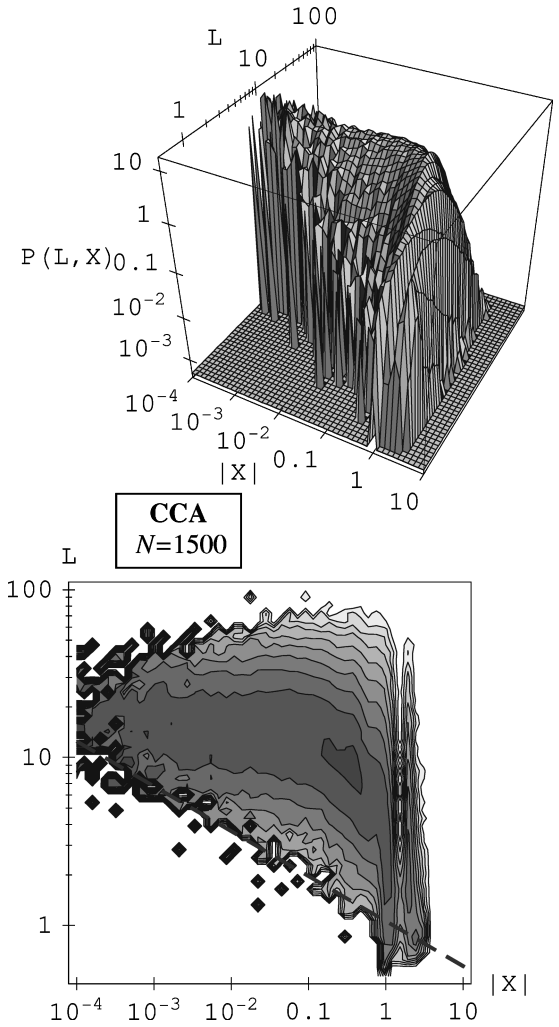

FIG. 3. Localization-length distribution $P(L,X)$ of eigenmodes for CCA clusters of $N=1500$ monomers each. The position of the lower-X cutoff l_X is qualitatively indicated by the dashed bold line.

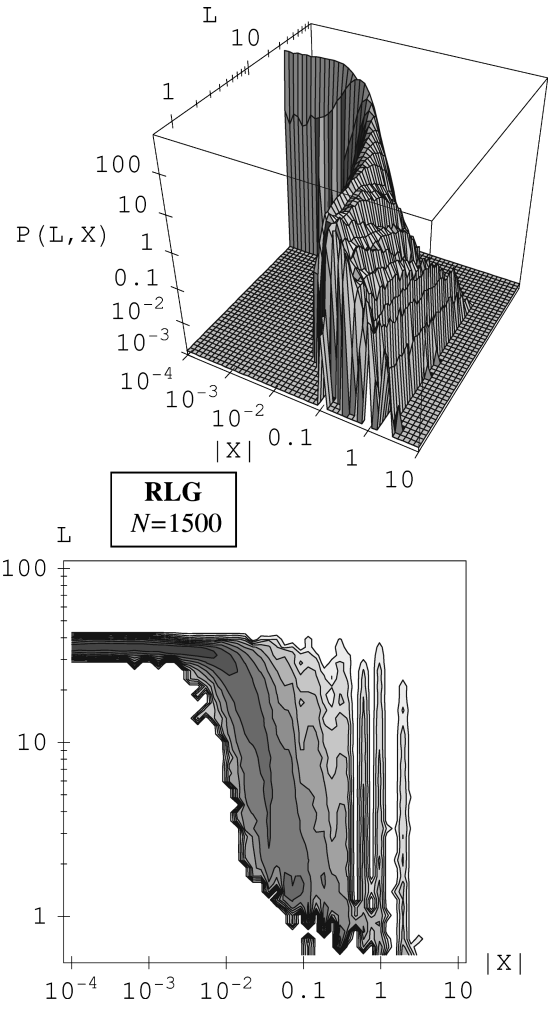

FIG. 4. Localization-length distribution $P(L,X)$ of eigenmodes for random lattice gas (RLG) clusters of $N=1500$ monomers each.

der from those of fractality. To do so, we consider the distribution function $P(L,X)$ for a disordered but not fractal system, a random lattice gas; see Sec. III A. The result of the corresponding computations for a RLG is shown in Fig. 4. As one can see, the distribution for $X \gtrsim 0.1$ is similar to that of a CCA (Fig. 3), characteristic of inhomogeneous localization. The major distinction from Fig. 3 is that the distribution in Fig. 4 shows the complete delocalization of the plasmons for $|X| \lesssim 0.01$ that appears in a narrow range. Such a delocalization is expected for the low-X part of the spectrum, i.e., at frequencies close to the plasmon resonance of the individual monomers. In contrast, there is no such delocalization for fractal (CCA) clusters, as seen in Fig. 3.

D. Dynamic form factor

As noted above in Sec. II B, the dynamic form factor $S(r,X)=\frac{1}{3}S_{\alpha\alpha}(r,X)$ is an important measure that determines the correlation of the eigenmode amplitudes, electromagnetic (polarization) fluctuations, electromagnetic absorption by the clusters, and energy loss of charged particles in cluster composites. The results of the computation of $S(r,X)$ for $N=1500$ CCA clusters are shown in Fig. 5. The most significant feature of this figure is a developed pattern of chaotic correlations. The ''landscape'' seen in Fig. 5 deserves the name of a ''devil's hill,'' where narrow regions of positive and negative correlation are interwoven resulting in a network reminding one of turbulence. Interestingly enough, the islands of correlation (either positive or negative) have almost vertical boundaries and the absolute values of the form factor for the adjacent regions are very close. This implies that the regions of positive and negative correlations form domains with narrow boundaries, resembling a binary (telegraph) noise superimposed on some smooth surface.

We emphasize that the changes of $S(r,X)$ are *not unstable* random fluctuations. The chaos seen in Fig. 5 is completely deterministic. Calculations with an independent statistical set of clusters of the same size reproduce the picture of Fig. 5. We also note that the distribution in Fig. 5 is not a spatial distribution, but rather a distribution in a combined coordinate-spectrum space, and it has no geometrical relation to the spatial randomness of the fractal clusters. This distribution is obtained by averaging over a large ensemble of clusters and is a characteristic ''fingerprint'' for the given type of clusters. The ensemble averaging does not smooth out the distribution.

The chaotic behavior of the dynamic form factor takes place for $|X|<1$, while for $|X|>1$ this function is dominated

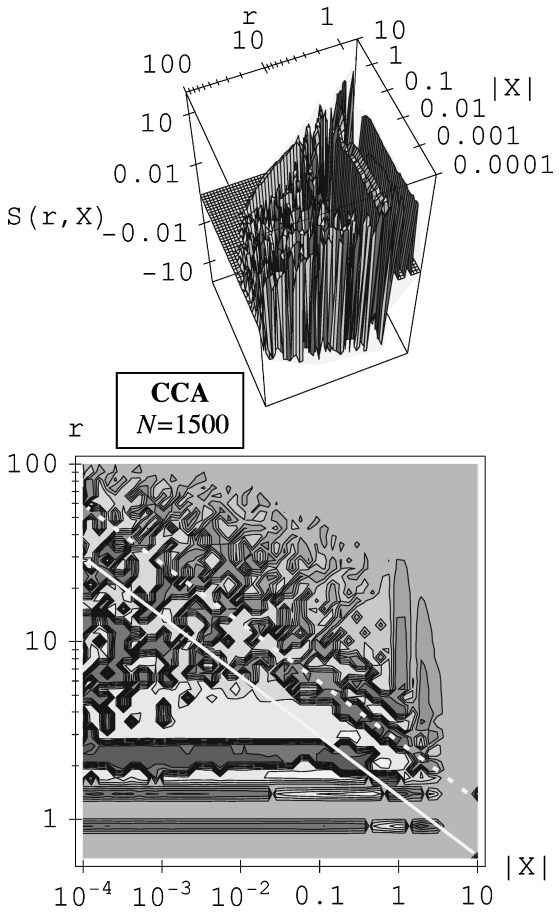

FIG. 5. Dynamic form factor $S(r,X)$ for $N=1500$ CCA clusters. A three-dimensional profile on double-logarithmic scale in r and X is shown in the upper panel and the corresponding contour map in the lower panel. The scale for $S(r,X)$ (the vertical scale) is pseudologarithmic to show simultaneously positive and negative values of $S(r,X)$. To obtain it, a small region of the plot for $|S(r,X)|\lesssim 10$ is removed. The function plotted is $\log_{10}(|S(r,X)|)\mathrm{sgn}[S(r,X)]$. The solid white line is the plot of Eq. (21) indicating the band of binary correlations. The dashed white line is the ternary correlation band given by Eq. (23).

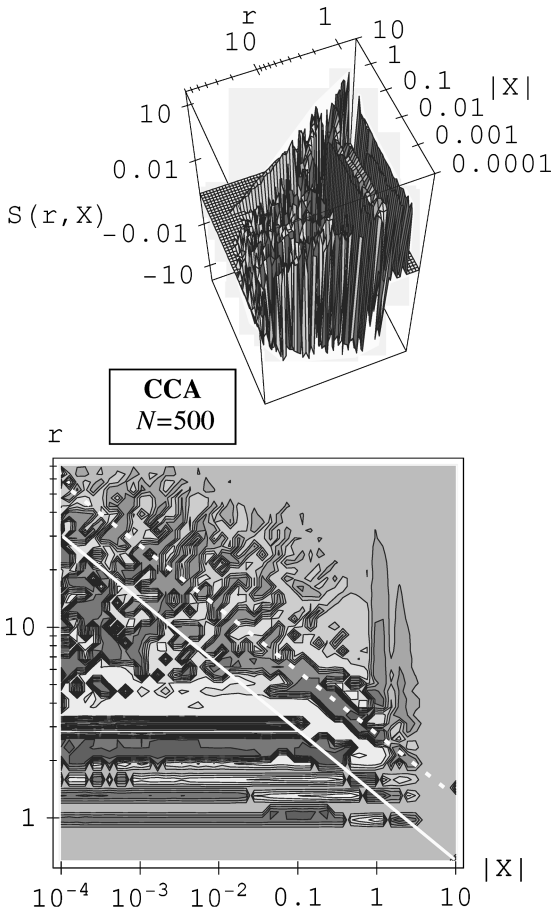

FIG. 6. Same as in Fig. 5, but for $N=500$. The r axis is scaled so that the total vertical size remains approximately double the mean gyration radius of the clusters.

by scaling ridges seen in Fig. 5 (extending vertically in the right lower corner of the bottom panel), corresponding to the similar structure in Fig. 3. This region of high eigenvalues is remarkable in many respects. In particular, the giant fluctuations of local fields and enhancement of optical nonlinearities are maximum in this region [7]. We will call this a scaling region because the correlation functions in this region are described by power dependences. To the left (to smaller eigenvalues), the scaling region borders the chaotic region.

The binary-approximation band of positive correlation of Eq. (21) is shown in Fig. 5 by the solid white line. For $0.1\lesssim|X|\lesssim 10$, this line coincides with the strongest positive-correlation features, but departs from them for $|X|\gtrsim 0.1$. The ternary correlation band of Eq. (23) is weaker, as one would expect. In the same region of $0.1\lesssim|X|\lesssim 10$, it fits well the corresponding band obtained numerically, as is evident from Fig. 5. We emphasize that the lines shown are given by Eqs. (21) and (23) and do not contain any adjustable parameters.

The prediction of scaling [see Eq. (16a)] is tested in Fig. 6, where the dynamic form factor for $N=500$ monomer CCA clusters is presented. One can see a remarkable general similarity between this figure and Fig. 5. However, fine details of the chaotic distribution are not completely reproduced. This suggests that the fingerprint in its fine details may be specific for the clusters of a given size. However, a study with much larger statistical sets and lattice sizes will be needed to arrive at a final conclusion regarding the scaling of the fine structure of the dynamic form factor. Another important conclusion that can be drawn from the comparison of Figs. 5 and 6 is that the eigenmodes in a wide spectral range fill the whole available space occupied by the cluster, limited by the total size of the cluster. This feature is characteristic of the inhomogeneous localization pattern and inconsistent with strong localization.

To distinguish between effects of fractality and nonfractal disorder, we compare below the above-presented results with the similar data for the RLG clusters, which are a random, but not fractal. The dynamic form factor for RLG ($N=1500$) is displayed in Fig. 7. One can see that there is a dramatic difference between fractal and non-fractal disordered (random) clusters. For the RLG clusters, some chaotic structure is seen only for $|X|\gtrsim 1$ (i.e., in the blue wing of the spectrum). In a wide region, for $|X|\gtrsim 0.001$, the dynamic form factor is dominated by the localized-plasmon branch seen extending diagonally in Fig. 7. There is a parallel band of negative correlation seen at smaller r. The binary-approximation prediction (Sec. II C) for the position of the

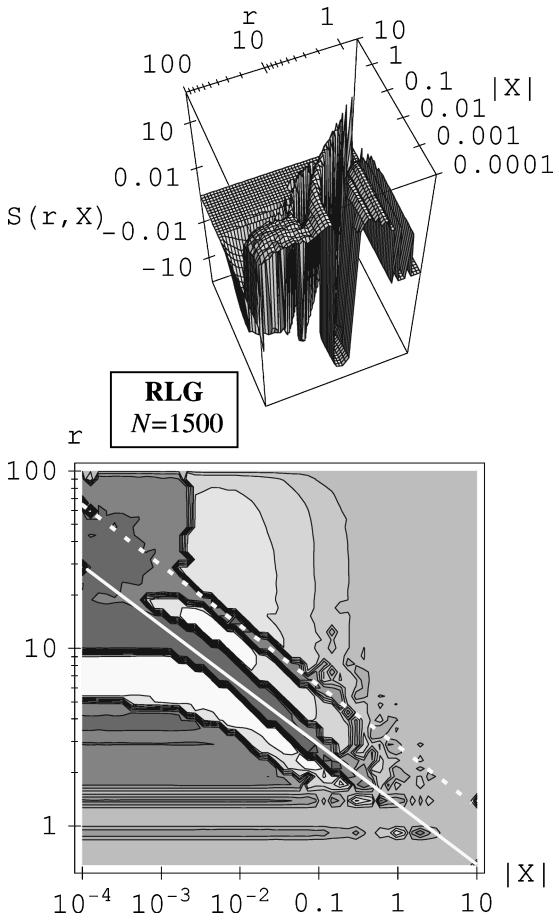

FIG. 7. Dynamic form factor $S(r,X)$ for $N=1500$ RLG clusters; otherwise similar to Fig. 5.

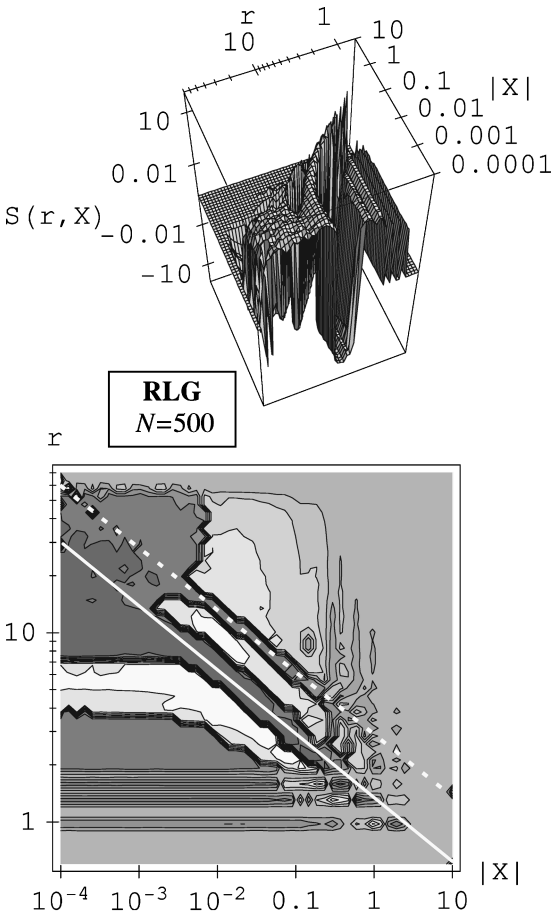

FIG. 8. Same as in Fig. 7, but for $N=500$. The r axis is scaled so that the total vertical size remains approximately double the mean gyration radius of the clusters.

positive-correlation band [see Eq. (21)] is shown in the figure by the white solid line. It is in very good agreement with the corresponding numerically obtained branch, as seen in Fig. 7, especially keeping in mind that there are no adjustable parameters. The ternary-approximation band of positive correlation is shown with the white dashed line and is also in a good agreement with the corresponding numerical feature. We note also that the correlation bands seen in Fig. 7 are due to localized plasmons. In contrast, a propagating wave would have resulted in a periodic pattern of parallel dark and white fringes.

Another important feature seen in Fig. 7 is the delocalization of the plasmons occurring at $X\approx 0.0025$. At smaller X, we see uniform positive correlation extending to the geometric limit of the clusters. This correlation implies that the polarization is uniform inside the clusters, thus all charges being localized at the cluster surface. This is clearly a transition to surface plasmons and it is a very sharp and well-defined transition. This result is in agreement with the localization-length data of Fig. 4. Similarly to the Anderson transition, this one occurs when the correlation radius of the wave increases. A principal distinction is that the plasmons are not running, but rather localized waves. Therefore, the scattering cross section for plasmons is not defined and the Anderson criterion is not applicable. Instead, the transition occurs when the radius of the localized plasmon becomes comparable to the size of the cluster, i.e., the delocalization criterion is

$$r\simeq |X|^{-1/3}\simeq R_c\,. \tag{24}$$

This delocalization has a mesoscopic nature because the size of the cluster is a governing parameter.

The transition frequency is determined by the equation $|X|\simeq R_c^{-3}\propto N^{-1}$. In such a way, for $N=500$ RLG clusters the transition is expected at $|X|\approx 0.008$; otherwise the correlation pattern should be similar to Fig. 7. To test these predictions, we present in Fig. 8 the numerical results for $N=500$ RLG clusters. As one can see, there is indeed a shift of the delocalization-transition frequency to $|X|\approx 0.008$, as expected. Except the transition position, there is a similarity between Figs. 7 and 8. In particular, the dominating bands of correlation are described by the same binary- or ternary-approximation formulas of Eqs. (21) and (23). This result strongly supports the mesoscopic, related to the total size of clusters, nature of the delocalization transition, distinct from the Anderson transition.

E. Intensity correlations

The sharp features seen in the devil's hill (Fig. 5) and in Figs. 7 and 8 are the boundaries where the dynamic form factor changes sign, i.e., correlation changes to anticorrelation. One can infer from these figures that the change of the phase of the polarization is quite abrupt. To further elucidate the relative importance of the phase and magnitude fluctua-

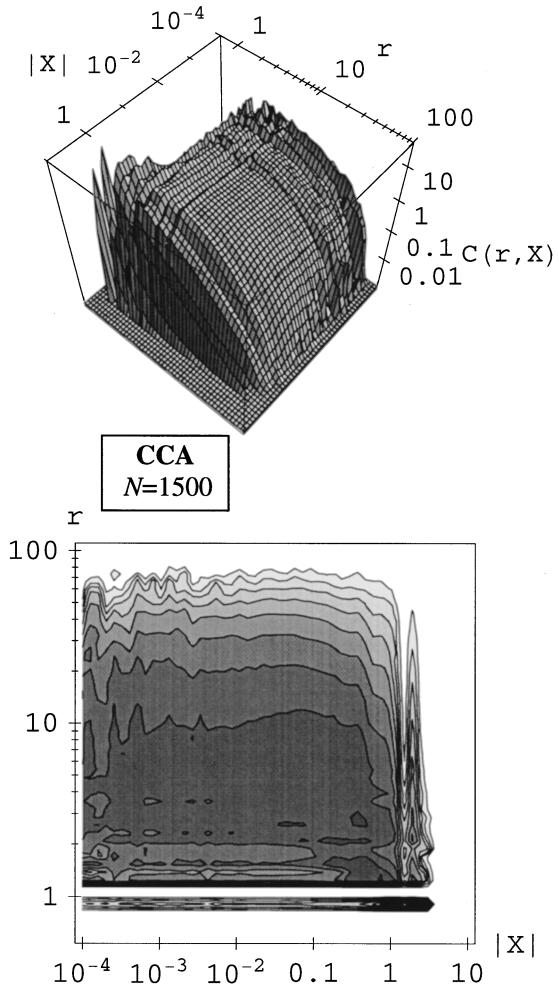

FIG. 9. Second-order correlation function $C(r,X)$ calculated for CCA clusters of $N=1500$ monomers each, averaged over ensemble of 300 clusters. The upper panel is the distribution plotted in the triple-logarithmic scale and the lower panel is the corresponding contour map.

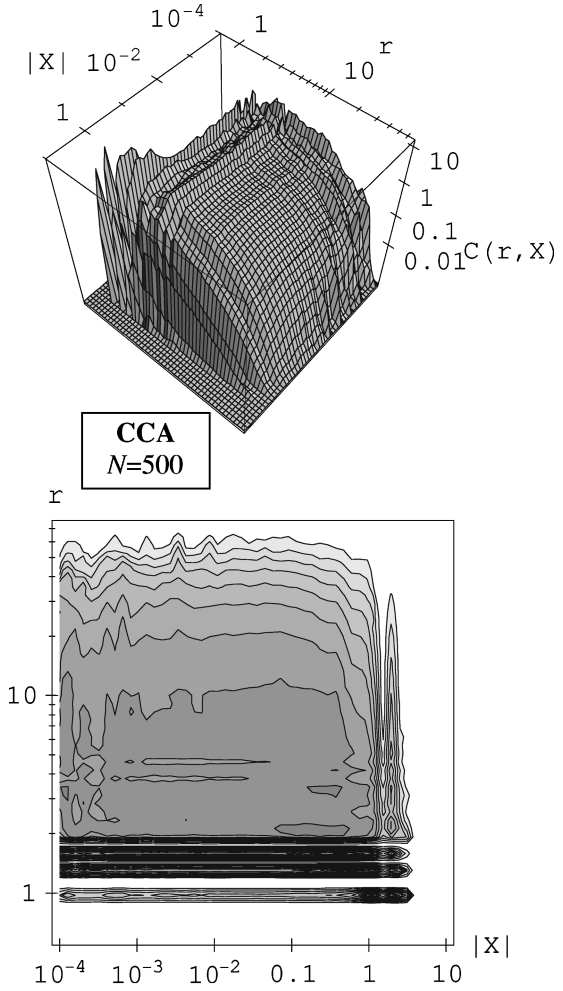

FIG. 10. Same as in Fig. 9, but for $N=500$.

tions of the local fields, we consider below the second-order (intensity) correlation function $C(r,X)$ of Eq. (10). This function is determined by the intensity correlations of the local fields and is insensitive to changes of their phases. The second-order correlator for CCA clusters is presented in Fig. 9.

The most pronounced difference of the second-order correlation (Fig. 9) from the dynamic form factor (Fig. 5) is its smoothness. This implies that the devil's hill landscape in Fig. 5 is created due to the abrupt, chaotic changes of the phases of the local fields, but not their magnitudes. This supports the qualitative picture of the amplitude correlation of the plasmons as a binary (''telegraph'') phase modulation superimposed on a very smooth envelope. Note that the intensity correlation is extended over the whole cluster and is limited by the cluster size, in contrast to the case of electron quantum-mechanical eigenproblems studied in Refs. [10,11].

The above-described behavior of intensity correlation is consistent with the inhomogeneous localization of the plasmons. In particular, it implies that the eigenmodes (the plasmons) behave in a certain sense as a gas, filling up the whole available volume of a cluster. A related property expected for such a localization pattern is scaling [see Eq. (16b)]. To test it, we consider the correlation function $C(r,X)$ for $N=500$, displayed in Fig. 10. Comparing this distribution with that of Fig. 9, we conclude that for $r \gg 1$ they are virtually indistinguishable. This result strongly supports the scaling predicted by Eq. (16b).

In Figs. 9 and 10, in the scaling region at $|X| \approx 2-3$, the power dependence of Eq. (17c) appears to hold. This conclusion is indicated by the straight lines of the slopes in the upper panels and by equidistant contours in the bottom panels of Figs. 9 and 10. Its presence implies that in this region the plasmons do not feel the external boundary of a cluster. This conclusion is consistent with the data derived above from the dynamic form factor.

The scaling can be conveniently traced in Fig. 11, where selected sections of the correlation function are shown. The scaling index found for $X \approx 2$ is $c=-2.1$, in a reasonable agreement with the value of -2.3 obtained in Ref. [22]. The size of the clusters in the present calculation is larger and the statistical accuracy is higher than in Ref. [22]. Note that $c=D_e-1$, where D_e is the Hausdorff dimension for the plasmons. Because this index is less than -1, it is impossible that such a correlation is possessed by any material distribution. The value obtained shows that the plasmons in the wings of the absorption contour (for $|X| \approx 1-3$) have an

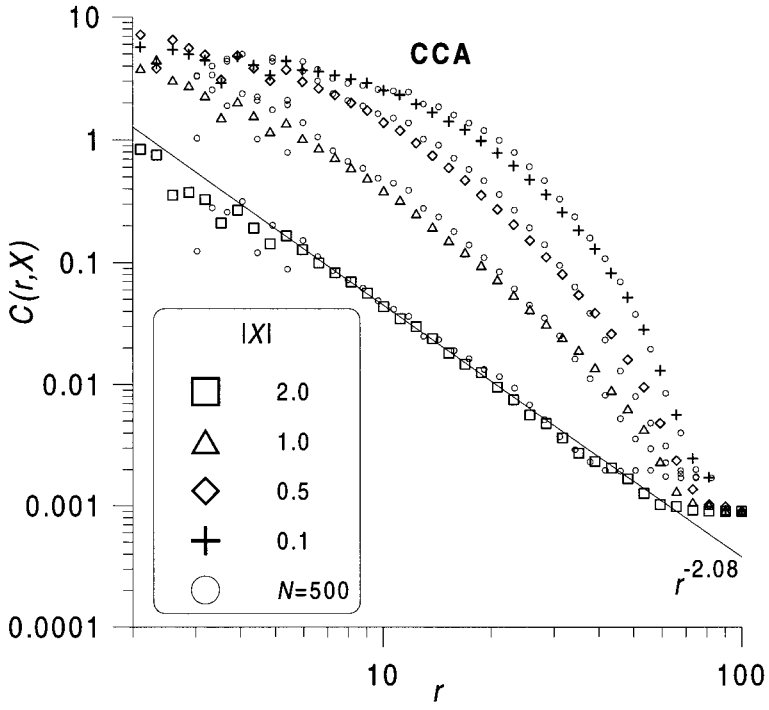

FIG. 11. Intensity-correlation function $C(r,X)$ for $N=1500$ CCA clusters for $X=-2.0,-1.0,-0.5,-0.1$, as indicated in the figure. The corresponding data for $N=1500$ are also shown by circles.

essential singularity at small r, supporting the conclusions of Ref. [22].

IV. DISCUSSION

In this paper we have investigated the localization properties, correlation, and fluctuations of the polar eigenmodes (plasmon excitations) of large clusters. This problem is mathematically equivalent to the Schrödinger equation eigenproblem [see Eq. (3)] for vector particles with a dipole interaction. The eigenmodes of the dipole-response problem (plasmons) map to the eigenstates of the corresponding quantum problem. We have found complex behavior of the eigenmodes and their correlators, including inhomogeneous localization and chaos of the individual eigenmodes, deterministic-chaotic behavior of the amplitude correlation function (the dynamic form factor) in fractal cluster-cluster aggregates, and the sharp delocalization transition for plasmons in a random lattice gas of spheres.

We have confirmed the earlier results of Ref. [22] that plasmons in fractal clusters do not obey either strong- or weak-localization patterns. Instead, a different pattern, inhomogeneous localization, takes place. At any frequency (parameter X) there coexist plasmons with dramatically different localization lengths, from the minimum scale l_X to the total size of the clusters R_c (see Secs. III B and III C). The individual plasmons, as illustrated by Fig. 1, are highly singular and chaotic, consisting of sharp peaks, strongly fluctuating in space. The plasmons with large coherence radius L_n actually consist of similar sharp peaks, separated by a distance of the order of the cluster size. In contrast, a delocalized wave in a nonfractal disordered system has a smooth envelope (as confirmed for the plasmons in a RLG).

The local fields in fractals induced by an external optical excitation also are also chaotic, consisting of sharp singular peaks strongly fluctuating in space. Despite their singular structure on the small scale, these fields are delocalized over the volume of the whole cluster, as seen in Fig. 2. When the polarization or frequency of the exciting wave change, the distribution of the local field intensity changes dramatically, supporting the general idea of (quantum) chaos in such systems. These features are in a good qualitative agreement with the experimental data of Ref. [6]; however, the conclusion of Ref. [6] that its experimental data support the strong localization hypothesis is not confirmed (see also Refs. [28] and [29]).

For the fractal CCA clusters, the distribution $P(L,X)$ of the plasmons over their localization lengths is extremely wide, supporting the coexistence of very different localization-length plasmons at virtually the same frequency as shown in Fig. 3, which is a signature of inhomogeneous localization. This distribution does not show any transition to localization or delocalization (weak localization) of the plasmons in the whole range of the spectral parameter X. The distribution spread in L is limited from below by $L \lesssim l_X$, where l_X scales with X as $l_X \propto |X|^{\lambda}$ with $\lambda \approx -0.25$. The scaling of this cutoff is attributed to the self-similarity (fractality) of the CCA clusters.

In contrast to this case of fractal clusters, the distribution $P(L,X)$ for disordered but not fractal RLG clusters demonstrates a sharp transition to delocalization for $|X|<0.01$, as seen in Fig. 4. This transition is confirmed and its mechanism is elucidated by considering the dynamic form factor for RLG clusters; cf. Fig. 7 and its discussion. For X greater than the edge of the delocalization transition ($X>0.0025$), the dynamic form factor is dominated by the branch of localized plasmons whose dispersion is in excellent quantitative agreement with the binary approximation formula of Eq. (21), as shown by the solid white line in Fig. 7. The first correction to the binary approximation, the ternary approximation of Eq. (23) (shown by the white dashed line), accurately describes the position of the weaker satellite band of positive correlation.

As discussed, due to the long range of the Coulomb interaction, the delocalization transition of the eigenmodes occurs when their coherence radius becomes comparable with the total size of the cluster; cf. Eq. (24). Consequently, distinct from the Anderson transition, the delocalization of RLG-cluster plasmons is a mesoscopic phenomenon, depending on the total size of the system. The underlying difference from Anderson localization is that the plasmons in the disordered clusters are not propagating waves; in particular, the scattering cross section that would play a major role in the Anderson localization is not defined for the plasmons. As follows from Eq. (24), for $N=500$ clusters compared with $N=1500$ clusters, the delocalization transition should happen at $|X|$ three times greater. This is indeed confirmed by the numerical data; cf. Fig. 8.

One of the most interesting and intriguing findings of the present study, in our opinion, is the ''turbulent,'' quasichaotic behavior of the dynamic form factor (i.e., the pair correlation function of the amplitudes of the plasmons) for the fractal CCA clusters; shown in Figs. 5 and 6. In contrast, such a behavior is absent for random, but not fractal, RLG clusters, cf. Figs. 7 and 8. The chaotic behavior of the dynamic form factor for the present dipolar problem is dramatically different from the short-range smooth correlation predicted in Ref. [10] and confirmed by Ref. [11] for electronic quantum-mechanical problems. Despite the chaotic structure of the dynamic form factor for fractal CCA clusters, it is well reproducible and demonstrates good statistical convergence under ensemble averaging. Therefore, it is actually an identifying characteristic (fingerprint) of a given type of cluster, depending on geometry and topology in particular. Whether the fingerprint is universal for clusters of the same type with different number of monomers is still a largely open question.

The chaotic behavior of the dynamic form factor for fractal clusters has also another signature. As seen from Figs. 5 and 6, the transition between the regions of positive and negative correlation is very abrupt. They strongly resemble in this respect domains of magnetization in a ferromagnet. The physical interpretation that we can give to this fact is that the binary approximation favors either the parallel on antiparallel alignment of the nearest excited regions (Sec. II C). Whether the geometry of these domains is itself fractal requires an additional investigation.

The chaotic behavior of the dynamic form factor for fractal clusters is a reflection of the underlying chaos of the eigenmodes (plasmons). These modes are chaotic in most of the spectral region (for $|X|\lesssim 1$). As the frequency moves away from the plasmon resonance, i.e., $|X|$ increases, chaotic behavior changes to scaling. The scaling manifests itself in smooth ridges seen in all of the distribution and correlation functions for CCA clusters at $|X|\gtrsim 1$. Despite the fact the scaling region is comparatively narrow on the logarithmic scale, it is important because it corresponds to the maximum enhancement of the optical responses [4,7].

ACKNOWLEDGMENTS

I am grateful to S. T. Manson and J. E. Sipe for many very useful discussions. I am thankful to W. H. Nelson for support and reading the manuscript. I appreciate comments by M. V. Berry on the results of this paper. I acknowledge with gratitude the invariable support and help by T. F. George. I thank L. N. Pandey for providing and adapting the computer routines for large-matrix diagonalization. I am grateful to Institute for Mathematics and its Applications for the hospitality during my participation in the program ''Mathematical Methods in Materials Science.'' I acknowledge grants from Georgia State University that allowed purchase of the state of the art computer equipment that made this investigation possible.

[1] E. M. Lifshitz and L.P. Pitaevsky, *Statistical Physics* (Nauka, Moscow, 1978), Pt. 2.
[2] J. Bauer, T.-M. Chang, and J. L. Skinner, Phys. Rev. B **42**, 8121 (1990).
[3] M. Moskovits, Rev. Mod. Phys. **57**, 783 (1985).
[4] M. I. Stockman, V. M. Shalaev, M. Moskovits, R. Botet, and T. F. George, Phys. Rev. B **46**, 2821 (1992).
[5] A. V. Butenko, P. A. Chubakov, Yu. E. Danilova, S. V. Karpov, A. K. Popov, S. G. Rautian, V. P. Safonov, V. V. Slabko, V. M. Shalaev, and M. I. Stockman, Z. Phys. D **17**, 283 (1990).
[6] D. P. Tsai, J. Kovacs, Z. Wang, M. Moskovits, V. M. Shalaev, J. S. Suh, and R. Botet, Phys. Rev. Lett. **72**, 4149 (1994).
[7] M. I. Stockman, L. N. Pandey, L. S. Muratov, and T. F. George, Phys. Rev. Lett. **72**, 2486 (1994).
[8] E. J. Heller, Phys. Rev. Lett. **53**, 1515 (1984).
[9] S. Tomsovic Phys. Rev. Lett. **77**, 4158 (1996).
[10] M. V. Berry, J. Phys. A **10**, 2083 (1977).
[11] V. I. Fal'co and K. B. Efetov, Phys. Rev. Lett. **77**, 912 (1996).
[12] T. C. Halsey, M. H. Jensen, L. P. Kadanoff, I. Procaccia, and B. I. Shraiman, Phys. Rev. A **33**, 1141 (1986).
[13] S. Russ and B. Sapoval, Phys. Rev. Lett. **73**, 1570 (1994).
[14] A. Petri and L. Pietronero, Phys. Rev. B **45**, 12 864 (1992).
[15] P. de Vries, H. De Raedt, and A. Lagendijk, Phys. Rev. Lett. **62**, 2515 (1989).
[16] A. Bunde, H. E. Roman, S. Russ, A. Aharony, and A. B. Harris, Phys. Rev. Lett. **69**, 3189 (1992).
[17] B. Sapoval, Th. Gobron, and A. Margolina, Phys. Rev. Lett. **67**, 2974 (1991).
[18] M. I. Stockman, T. F. George, and V. M. Shalaev, Phys. Rev. B **44**, 115 (1991).
[19] V. A. Markel, L. S. Muratov, and M. I. Stockman, Zh. Éksp. Teor. Fiz. **98**, 819 (1990) [Sov. Phys. JETP **71**, 455 (1990)]; V. A. Markel, L. S. Muratov, M. I. Stockman, and T. F. George, Phys. Rev. B **43**, 8183 (1991).
[20] S. Alexander and R. Orbach, J. Phys. (France) Lett. **43**, L625 (1982).
[21] M. I. Stockman, L. N. Pandey, L. S. Muratov, and T. F. George, Phys. Rev. B **51**, 185 (1995).
[22] M. I. Stockman, L. N. Pandey, and T. F. George, Phys. Rev. B **53**, 2183 (1996).
[23] P. Meakin, Phys. Rev. Lett. **51**, 1119 (1983).

[24] M. Kolb, R. Botet, and R. Jullien, Phys. Rev. Lett. **51**, 1123 (1983).

[25] J. Cullum and R.A. Willoughby, *Lanzcos Algorithms for Large Symmetric Eigenvalue Computations* (Birkhauser, Basel, 1985).

[26] V. M. Shalaev, R. Botet, and A. V. Butenko, Phys. Rev. B **48**, 6662 (1993).

[27] Yu. E. Danilova, A. I. Plekhanov, and V. P. Safonov, Physica A **185**, 61 (1992).

[28] M. I. Stockman, L. N. Pandey, L. S. Muratov, and T. F. George, Phys. Rev. Lett. **75**, 2451 (1995).

[29] M. I. Stockman and T. F. George, Phys. World **7**, 27 (1994).